Bistatic Radar Positioning of a Moving Target, Using Only Range and Range-Rate Measurements

ITZIK COHEN
NADAV LEVANON, Life Fellow, IEEE
Tel Aviv University, Tel Aviv, Israel

Of the many applications of bistatic (BS) radars, this article addresses the possibility to replace a monostatic radar with its highly directive antenna, with a coherent BS radar using a single short baseline between the transmitter and the receiver and no direction measurements. The method applies to a moving target and requires both *range* and *range-rate* BS measurements. Theory and field-test results demonstrate, on a two-dimensional scene, how several consecutive pairs of BS *range* (r) and *range-rate* ($\dot{r}$) measurements of a moving target can provide the target's position, velocity, and heading (x, y, v_x, v_y). In a three-dimensional scene, with five estimated target parameters (x, y, h, v_x, v_y), a second receiver is needed, not in-line with the original baseline. The (r, $\dot{r}$) measurements distinguish the suggested concept from most other multistatic radars as well as the well-known multilateration positioning or interferometric angle-of-arrival estimation.

Manuscript received 11 May 2022; revised 6 August 2022; accepted 25 August 2022. Date of publication 30 August 2022; date of current version 12 April 2023.

DOI. No. 10.1109/TAES.2022.3202758

Refereeing of this contribution was handled by M. Gashinova.

Authors' address: The authors are with the Electrical Engineering – Systems Department, Tel Aviv University, Tel Aviv 6997801, Israel, E-mail: (levanon@tauex.tau.ac.il; bitzikc@gmail.com). *(Corresponding author: Nadav Levanon.)*

I. INTRODUCTION

Antennas, phase-array, or the rotating aperture are usually the largest and most expensive components of a radar system. Good direction resolution provides simple, quick, and effective positioning of a target, thanks to the perpendicular intersection between the radial direction line and the iso-range circle or sphere. Pencil-beam antenna also provides power gain, but there are other techniques to increase the energy on the target. In a limited number of cases, the concept described here can provide an alternative to antennas' main property—good target direction estimation. The main limitations of the concept are applicability only to moving targets observed by coherent radar and dependence on the geometry of the scene. Other restrictions will become evident from the description.

This article tells the story of a low-budget field experiment of a bistatic (BS) radar that ended up providing more significant results than originally envisioned. The BS field experiment was discussed in detail in [1]. It involved a 9-GHz, 1-W, periodic phase-coded continuous wave (CW) radar, and a 100-m baseline. The antennas had approximately $17^0_{\mathrm{W}} \times 25^0_{\mathrm{H}}$ beamwidth. To allow offline processing, high-rate raw digital data (I & Q samples) were continuously recorded. In [1], the targets were cars moving on a known road, within a range limit of 400 m. The original purpose was to study optimal processing and the delay-Doppler performances attainable with that particular periodic CW signal.

The stored I & Q samples enticed more browsing, which revealed an additional recorded scene, involving a low-flying airliner at a distance of 3.5 km. That prompted a new task—determine the aircraft's track parameters (horizontal position, velocity, and direction) using a sequence of BS (r, $\dot{r}$) measurements, obtained during a short aircraft track, lasting 2.4 s. Measuring BS $\dot{r}$ requires a *common frequency*, namely synchronization of the receiver's master oscillator to the transmitter's one. In our BS radar, phase-locking the receiver's oscillator to the carrier of the received direct-path, in addition to phase-locking and compensation of period interval time drift, provided the synchronization. Using a CW signal helps that approach. However, other methods of frequency synchronization have been reported [2], [3], [4], like using GPS disciplined oscillators or connecting the transmitter and the receiver by optical fiber. Our approach does not require *common time*, which is more difficult to obtain.

BS and multistatic radar is a fast expanding topic, spanning many applications, problems, methods, and geometries. Correspondingly, the literature is vast. Measurements may include delay only, Doppler only or both. Baselines and ranges may span from many kilometers [5] to a few meters [6] ([5] and [6] contain valuable bibliography.) The signal may come from sources of opportunity (passive BS), or from a dedicated transmitting element of the BS system (active BS). The passive BS field is especially expanding in both applications (area security, automotive, integrated

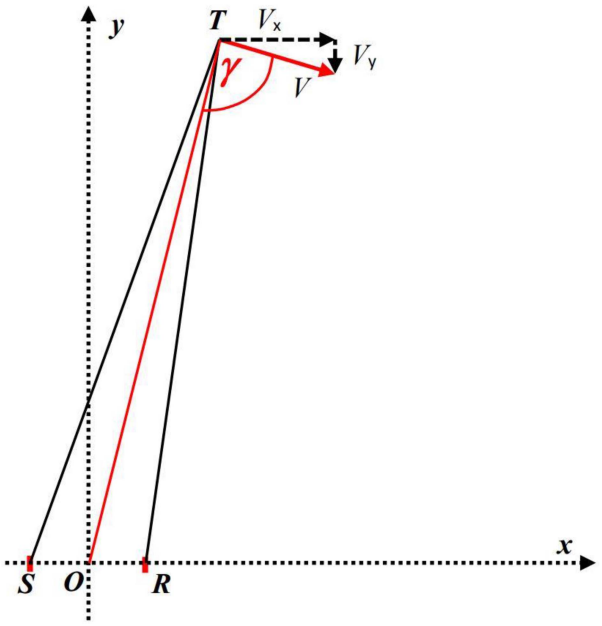

Fig. 1. 2-D geometry of the BS radar.

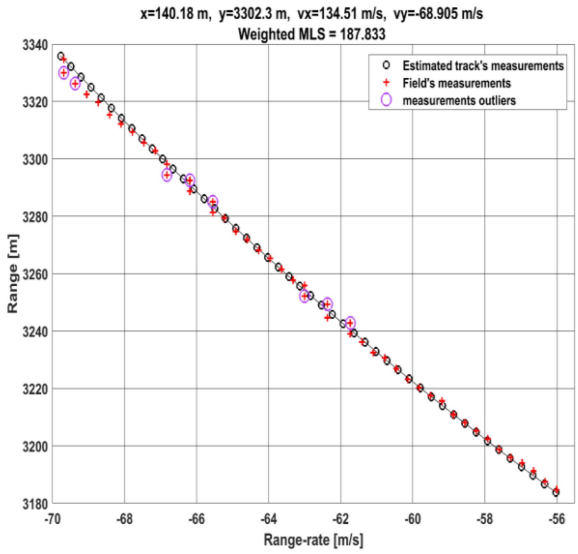

Fig. 2. $N = 47$ measured pairs of range versus range rate, compared to the best matched simulated pairs.

sensing, and communication (ISAC) and many more) and signal sources (FM broadcast, DVB-S, Wi-Fi, OFDM, G5, GPS, etc.). Most signals of opportunity are not optimized for radar and are also changing with time, which makes classical radar processing, like matched filters and Doppler processing, less effective and more difficult to implement.

Of the many BS radar slots, our system best fits into the following one: (a) system—active stationary coherent BS; (b) measurements—delay and Doppler, with short coherent intervals and many consecutive repetitions; (c) purpose—locate moving targets with a narrow range and range-rate resolutions; (d) baselines—relatively short; and (e) antennas—relaxed directivity demands. This characteristic is closer to monostatic radar than to passive BS radar. The main difference from a monostatic radar is the baseline(s) separating the transmitter from the receiver(s). This difference is what enables target positioning without direction measurements, and it also encourages the use of CW waveforms.

II. GEOMETRY AND DEFINITIONS

Our discussion begins with the 2-D geometry because the field experiment utilized a single baseline. The 2-D geometry allows estimating four target parameters (x, y, v_x, v_y), for any assumed target's altitude h. The 2-D geometry can demonstrate the important role of the range-rate $\dot{r}$ measurement in position estimation. It can also point out unfavorable scenes, where the geometric dilution of precision (GDOP) [7], [8], [9] is poor. Analysis of a 3-D scene, using simulations, will show that the second receiver, not aligned with the first baseline, enables estimating the missing target's fifth parameter, i.e., its altitude.

Fig. 1 displays a sketch of the 2-D scene. It also helps define the various parameters. The three participating elements are: the source (transmitter) S, the target T, and the receiver R. Their coordinates are

$$\boldsymbol{S}(x_s, 0), \ \boldsymbol{R}(x_r, 0), \ \boldsymbol{T}(x, y) \ \text{where } x_s = -d/2, \ x_r = d/2.$$

The three points ($\boldsymbol{S}$, $\boldsymbol{T}$, $\boldsymbol{R}$) define the 2-D plain, which does not necessarily coincide with a flat Earth surface. Without loss of generality, the baseline connecting S and R is aligned with the x-axis. Its length is d and it centers on the origin $\boldsymbol{O}(0, 0)$. We assume a straight-line target's track, centered at T and aligned with the velocity vector V. We also assume constant target's velocity components v_x and v_y. $\boldsymbol{\gamma}$ is the angle between the velocity vector and the BS bisector.

A sequence of N simultaneous pairs of BS *range* and *range-rate* measurements were obtained, equally spaced, at sampling instances $t(n)$

$$t(n+1) - t(n) = t_s, \quad n = 1, 2, \ldots, N. \tag{1}$$

Using an odd N will place the center of the track at $t[(N+1)/2] = 0$.

The variable t_s represents the time interval between consecutive, independent measurements of the BS range, and range-rate measurements. t_s is also the duration of the *coherent processing interval* (CPI) that results in a delay/Doppler (range/range-rate) map. Namely, for every t_s, Fig. 3 is produced.

The N BS range measurements are related to the positions of the source, receiver, and moving target

$$r(n) = \tfrac{1}{2}\left[|\bar{r}_S - \bar{r}_T(n)| + |\bar{r}_T(n) - \bar{r}_R| - d\right] \tag{2}$$

where $\bar{r}_s$ is a vector containing the coordinates of the subscript (e.g., source). The coordinates are

$$\bar{r}_S = (x_S, y_S), \ \bar{r}_R = (x_R, y_R), \ \bar{r}_T(n) = (x + v_x t(n), \ y + v_y t(n)).$$

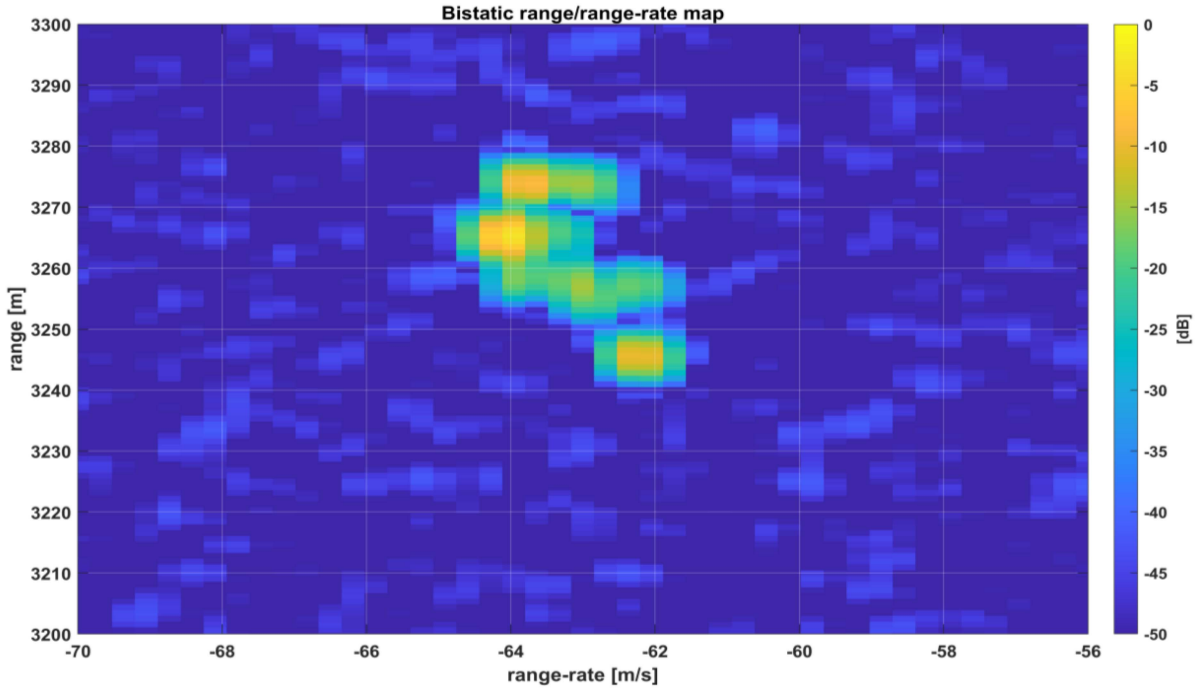

Fig. 3. Radar's range versus range-rate display of the airliner, taken near the middle of the track.

In more details

$$r(n) = \frac{1}{2}\left[\left(x + v_x t(n) - x_s\right)^2 + \left(y + v_y t(n)\right)^2\right]^{1/2} + \frac{1}{2}\left[\left(x + v_x t(n) - x_r\right)^2 + \left(y + v_y t(n)\right)^2\right]^{1/2} - \frac{d}{2}. \tag{3}$$

Subtracting $d/2$ reflects the actually measured delay difference between the arrival times, at the receiver, of the target reflection and the transmission through the direct path along the baseline.

The BS range rate can be calculated at the receiver as time derivatives of (2), using the estimated parameters $(\hat{x},\ \hat{y},\ \hat{v}_x,\ \hat{v}_y)$, obtained at the previous iteration. ($\hat{x}$ implies an estimate of x.)

$$\dot{\hat{r}}(n) = \frac{\partial \hat{r}(n)}{\partial \hat{\bar{r}}_T^{\dagger}(n)} \frac{\partial \hat{\bar{r}}_T(n)}{dt} = \left[\frac{\hat{x} + \hat{v}_x t(n) - x_S}{2\left|\bar{r}_S - \hat{\bar{r}}_T(n)\right|} + \frac{x + \hat{v}_x t(n) - x_R}{2\left|\hat{\bar{r}}_T(n) - \bar{r}_R(n)\right|}\right]\hat{v}_x + \left[\frac{\hat{y} + \hat{v}_y t(n) - y_S}{2\left|\bar{r}_S - \hat{\bar{r}}_T(n)\right|} + \frac{\hat{y} + \hat{v}_y t(n) - y_R}{2\left|\hat{\bar{r}}_T(n) - \bar{r}_R(n)\right|}\right]\hat{v}_y. \tag{4}$$

The positioning algorithm, at each iteration step, will have to generate N corresponding *estimated* BS range measurements, based on the estimated four parameters $(\hat{x},\ \hat{y},\ \hat{v}_x,\ \hat{v}_y)$ reached in the previous iteration. That estimated BS range is given by an equation similar to (3)

$$\hat{r}(n) = \frac{1}{2}\left[\left(\hat{x} + \hat{v}_x t(n) - x_s\right)^2 + \left(\hat{y} + \hat{v}_y t(n)\right)^2\right]^{1/2} + \frac{1}{2}\left[\left(\hat{x} + \hat{v}_x t(n) - x_r\right)^2 + \left(\hat{y} + \hat{v}_y t(n)\right)^2\right]^{1/2} - \frac{d}{2}. \tag{5}$$

In practice, the receiver derives the actual $\dot{r}$ measurement from the Doppler shift of the target's reflection. This requires synchronization between the master oscillators in the transmitter and receiver, which is not a trivial task. Calculating an estimated $\dot{\hat{r}}$ measurement can be approximated by numeric derivatives for each $t(n)$, using two additional estimated BS *range* measurements, one, labeled $\hat{r}_b(n)$ is calculated at $t(n) - \Delta t$. The other, labeled $\hat{r}_a(n)$, is calculated at $t(n) + \Delta t$, where $\Delta t << t_s/2$. The resulting simulated *range-rate* measurement is obtained from the early and late simulated *range* measurements as follows:

$$\dot{\hat{r}}(n) = \frac{1}{2\,\Delta t}\left[\hat{r}_a(n) - \hat{r}_b(n)\right]. \tag{6}$$

We now have a sequence of N *measured* pairs $r(n)$, $\dot{r}(n)$, $n = 1, 2, \ldots, N$ and a sequence of N *estimated* measurement pairs $\hat{r}(n)$, $\dot{\hat{r}}(n)$, $n = 1, 2, \ldots, N$, taken or estimated at the same time instances $t(n)$, $n = 1, 2, \ldots, N$. Our choice of the final estimate of the four

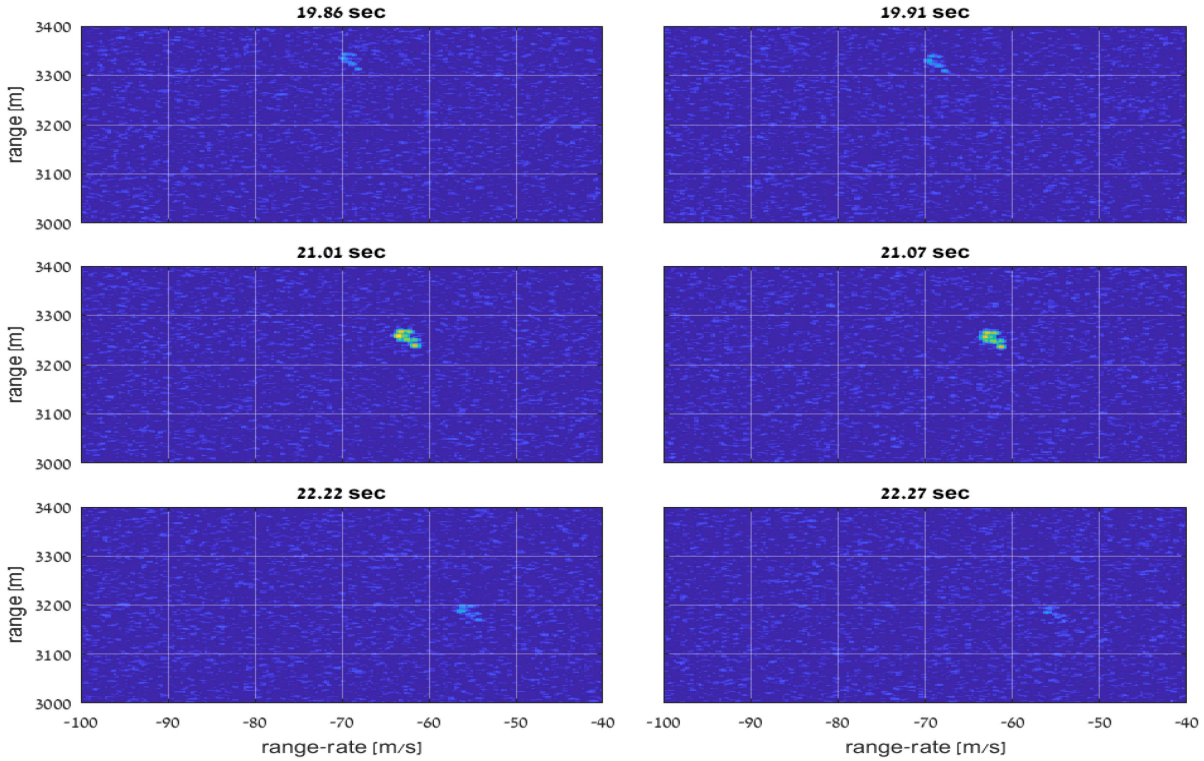

Fig. 4. Six snapshots of the radar's range versus range-rate display (the color bar of Fig. 3 applies).

target parameters $\hat{\theta} = (\hat{x}, \hat{y}, \hat{v}_x, \hat{v}_y)$ will be the one that will minimize F, the sum of weighted distances squared between corresponding points on the *range* versus *range-rate* plane

$$F = \sum_{n=1}^{N} \left\{ [r(n) - \hat{r}(n)]^2 + w^2 \left[\dot{r}(n) - \hat{\dot{r}}(n) \right]^2 \right\} \quad (7)$$

where w is a weight factor, multiplying the range-rate difference. How to choose w will be explained following a display of results from the field experiment.

Seeking the minimum of the 4-D surface function F, in the 4-D space, whose four axes are (x, y, v_x, v_y), is an optimization process, of which there are many methods, most of them iterative. Looking for the best method for our application is beyond the scope of this article.

III. FIELD EXPERIMENT RESULTS

Fig. 2 displays $N = 47$ *range* versus *range-rate* pairs (red "+" markers), measured in the field experiment, with the BS radar described in [1]. The circled $\oplus$ marker indicates a measurement that can be labeled as "outlier." However, because of their relatively small additional deviations, the outliers were not excluded from the estimation process. The weighted minimum least-squares algorithm produced the simulated measured pairs (displayed as black "o" markers). The resulting estimated track parameters appear in the drawing's title. The weight factor w, used in (7), equals approximately the measurements ratio at the track's center, $w = 50 \approx r(N/2)/\dot{r}(N/2) = 3260/64$.

Going a step backward, Fig. 3 is a snapshot of the radar's *range* versus *range-rate* output, taken near the center of the track. The radar's resolution cell is 0.94 m in *range* and 0.32 m/s in *range-rate*. Because the target was a large airliner, it occupied many cells, at varying intensities. In Fig. 3, the target's range spreads over approximately 30 m, and the range-rate spreads over about 3 m/s. To reduce errors, a dominant scatterer has to be chosen as the representative. The choosing criterion was a strong scatterer that appears in most of the other target's snapshots in the track. The chosen scatterer appears in Fig. 3 at (−64 m/s, 3265 m).

It will be impractical to show all 47 snapshots of the track, thus, in Fig. 4, 6 snapshots are displayed (1,2, 23,24,46,47). In many snapshots, the airliner intensity pattern resembles the pattern in Fig. 3, and the representative scatterer was easily identified.

The four estimated track parameters produce a track estimate, plotted in Fig. 5. Note that the two subplots are sections of the same map, with a large part of the y-axis ($50 < y < 3200$) omitted. The good agreement, seen in Fig. 2, between the N actual measurements of r and of $\dot{r}$ and the N estimated measurements, increases the confidence in the assumption of an airplane flying along a straight horizontal line at a constant velocity, at least for the 2.4 s of the recorded track. Allowing more parameters, e.g., the track altitude h, should not be ruled out, especially as long as the number of measurements accedes, by far, the number of unknowns. Adding h implies the 3-D geometry, which will require one more receiver and more processing power.

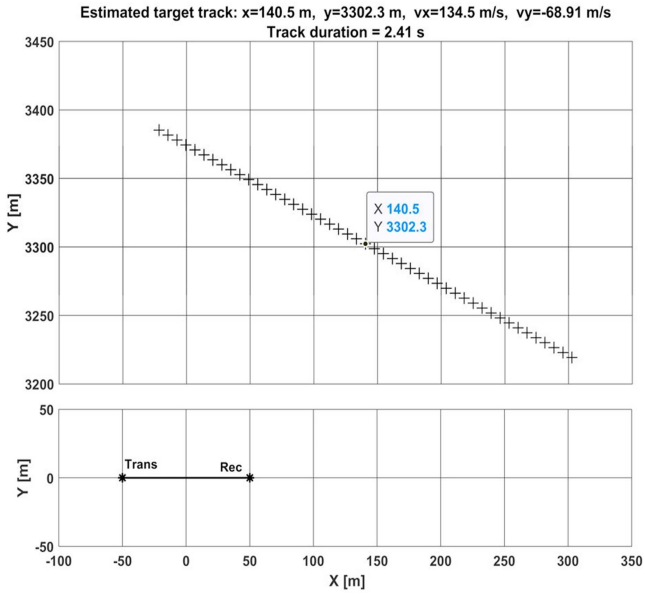

Fig. 5. Estimated target's track in the S-T-R plain.

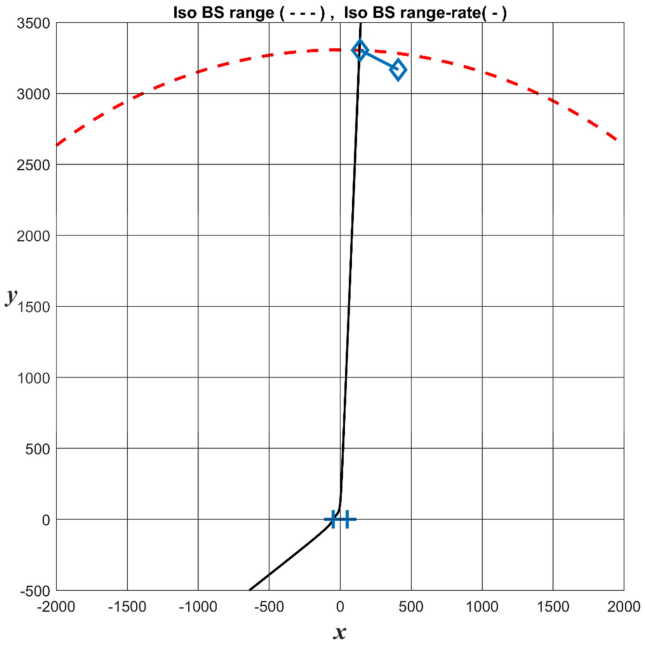

Fig. 6. Intersection between the BS iso-range (dash, red) and iso-range-rate (solid, black) contours, in the field experiment. Also shown is the velocity vector (solid, blue, and diamond markers).

IV. UNFAVORABLE 2-D SCENARIOS

Regarding the position $(x,\ y)$ estimate, there are multistatic radar systems that can position a target without using high directivity antennas. However, in the 2-D geometry, they usually require three or more baselines, created by three or more operating receivers, and be able to obtain the difference in the times of arrival, at the different receivers. To get a low geometric delusion of precision (GDOP), the baselines should have different aspect angles with respect to the transmitter and the target. Our approach, which uses both BS *range* and BS *range-rate* measurements, requires one baseline in the 2-D geometry, and two baselines in the 3-D geometry. *Range-rate* limits the use to moving targets and requires Doppler processing, which inherently lowers clutter returns, as is evident from the background in Figs. 3 and 4. Target's range sidelobes are also absent, thanks to the transmitted signal, which exhibits perfect periodic autocorrelation.

Our approach is also sensitive to GDOP, and some unfavorable scenarios are revealed in this section. In conventional monostatic radar that uses a good antenna, the GDOP is inherently optimal because the direction line will always be perpendicular to the iso-range circle. The main question in our system is how the BS iso-*range* (an ellipse) and iso-*range-rate* contours intersect. The answer will depend on the geometry, including the target's velocity direction. Fig. 6 gives an answer for the field experiment scene, showing an almost perpendicular intersection. Also shown are the baseline (blue + markers) and the velocity vector (blue diamond markers) connecting the target's present position to where it will be after 2 s.

The iso-range-rate contour will be different for a different target movement direction. We will demonstrate it by a second simulated example, with the same target position and velocity magnitude, but a different velocity direction. In that

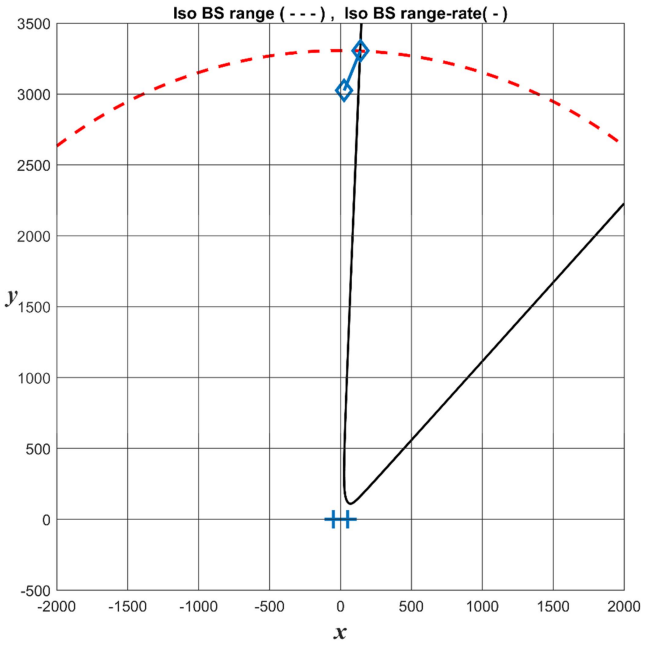

Fig. 7. Intersection between the BS iso-range (dash, red) and iso-range-rate (solid, black) contours, in the second synthetic scene.

second scene, the target's parameters and the corresponding BS measurements are

$$\begin{aligned}(x,\ y,\ v_x,\ v_y) &= (140\,\text{m},\ 3305\ \text{m},\ -57\ \text{m/s},\\ &\quad -140\ \text{m/s}) \rightarrow (r,\ \dot{r})\\ &= (3257\ \text{m},\ -142.25\ \text{m/s})\,.\end{aligned}$$

Fig. 7 displays the resulting contours of the iso-range and iso-range-rate measurements. Comparing the contours in Figs. 6 and 7, note that despite the different directions

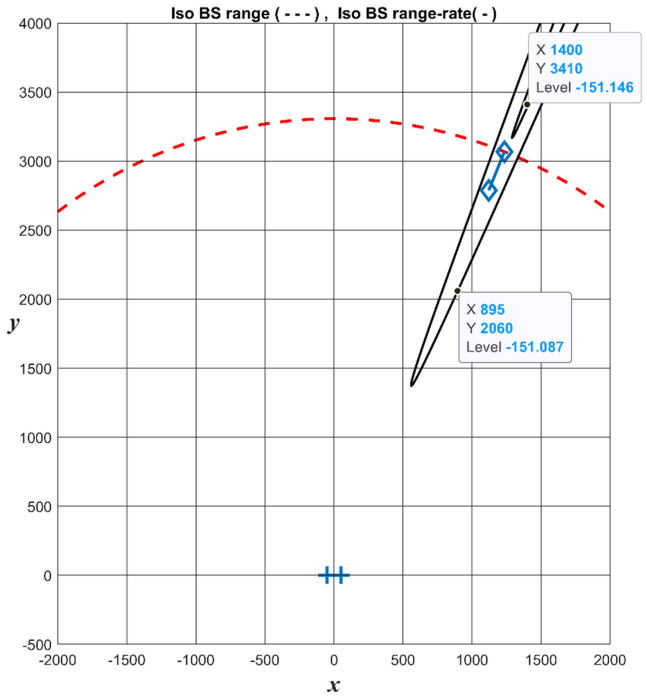

Fig. 8. Unsolvable scene where the target moves along the BS bisector. The data point "Level" is the value, in m/s, of the iso-range-rate contour.

of the velocity vector, the intersection at the target's location (140 m, 3305 m) is very similar, and remains near-perpendicular. The differences in the range-rate contour are more evident near the baseline (the hyperbola does not cross the baseline) and in the second arm of the hyperbola. Fig. 7 hints at an ambiguous second intersection between the contours, at an azimuth angle different by about 35° from the true intersection. While the antennas' beamwidth do not have to provide directivity, they will have to resolve this kind of ambiguity. If the antenna beam covers the false target but does not include the true target, it will not receive a reflected signal. The two arms of the hyperbola will get closer to each other as the target's moving direction points more toward, or away from the baseline center. This will cause the two intersections to happen within the antenna beam, preventing a decision on the true one. Fig. 8 describes such a scene. Beyond a certain closeness, the iso-range-rate hyperbola will not even intersect the iso-range ellipse. The conclusion is that the suggested positioning approach will not work when the target moves along the BS bisector.

V. FLAW OF FITTING A 2-D SCENE INTO 3-D REALITY

The target of opportunity in the field experiment happened to be an airliner, probably on a training flight above the sea, slightly off the coastline. However, even a training flight will not take place at zero altitude ($h = 0$). That raises the question: can the presently assumed constant altitude h, be added as a fifth estimated parameter. The three elements of our system are: transmitter (S), target position at the center of the track (T), and receiver (R). These three locations define a plain. As long as the target's track remains on that plain, the problem remains a 2-D scene. However, that plain can rotate, like a door, around the hinge, defined by the baseline. In the field experiment, the short track probably remained in that plain; hence, the estimated solution should be indifferent to the target's altitude. A different assumed value of h will mainly alter the estimated values of the horizontal position parameters (x, y), of the track center, so that $\sqrt{x^2+y^2+h^2}$remains unchanged. Table I demonstrates the MLS solution with two different assumed target altitudes: 0 and 600 m.

TABLE I
Influence of the Assumed Track Altitude

h [m]	x [m]	y [m]	vx [m/s]	vy [m/s]	$\sqrt{x^2+y^2+h^2}$	Minimum Weighted LS
0	140.5	3302.3	134.5	−68.91	3305.3	188.553
600	84.8	3249	135.1	−67.75	3305.0	188.3474

TABLE II
Estimation Dependence on Assumed Target's Altitude in a Noise-Free Simulation With 2 Receivers

Assumed	Estimated					Minimum Weighted Least Squares MWLS
h [m]	x [m]	y [m]	vx [m/s]	vy [m/s]	$\sqrt{x^2+y^2+h^2}$	
600 (true)	85	3249	136	−68	3305.0	0
500	93.0	3265.0	136	−68	3304.4	45.21

Table I confirms the indifference to the target's altitude by showing that the two solutions are of equivalent quality. The two different solutions reached the same depth (minimum) of weighted least squares (MWLS ≈ 188), implying the same quality of the match between the field experiment and the assumed measurements. In addition, as predicted, the two values of $\sqrt{x^2+y^2+h^2}$are practically equal.

To create some dependence on the target's altitude, it is necessary to prevent the plain, defined by the baseline and the target, from freely rotating around the "hinge" defined by a baseline, along the line $(y = 0)$. One way is to add a second receiver and place it *off* that line, namely where $(y \neq 0)$. Furthermore, not necessarily at zero altitude. In the following noise-free simulation, the second receiver was placed at $R_2(x = d/2,\ y = -d,\ z = 30\ m)$.

In a noise-free simulation, when the "true" target's altitude is assumed, it is expected that the estimation will converge when the MWLS $= 0$. Table II shows that when the assumed altitude was off by 100 m, the estimation converged to different four parameters, and the MWLS, at convergence, did not reach zero. This suggests that when the target's altitude parameter is not assumed but estimated, and if the SNR is high, the iterations will eventually converge to the correct altitude estimation. Two receivers can be placed in an endless number of combinations, which suggests further studies. Fig. 9 displays the 3-D simulation scene, with its two receivers, and the target parameters used in Table II (at $h = 600$ m).

VI. COMMENTS

A. Tradeoffs of the Measurements Sampling Interval

The variable t_s, which appeared in (1), represents the time interval between consecutive, independent

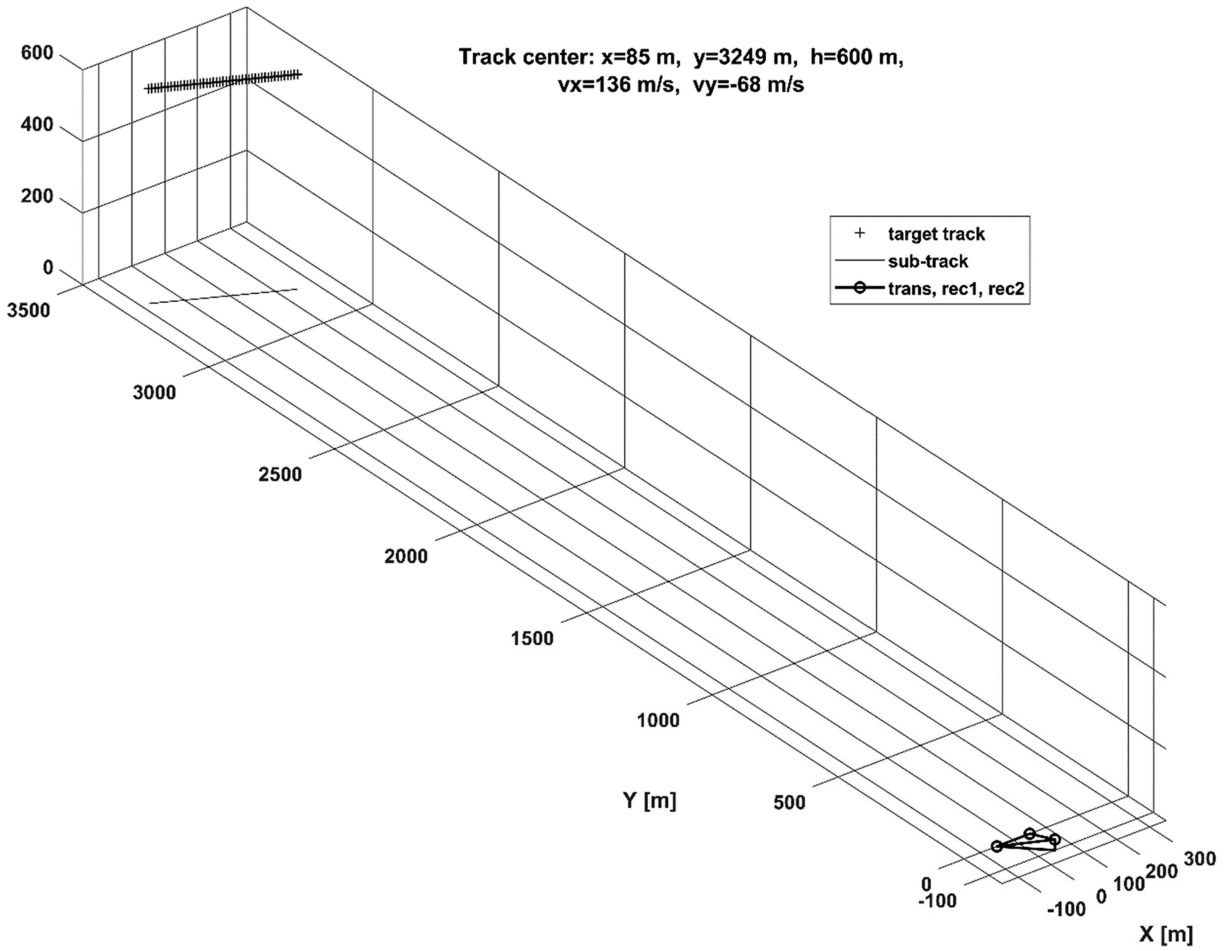

Fig. 9. 3-D simulated scene, employing two receivers.

measurements of the BS range and range-rate measurements. The t_s interval was set in the field experiment [1] to be 50 ms, which was the CPI of the Doppler measurement. Periodic CW waveform allowed continuous transmission between consecutive measurements. Increasing t_s, by increasing the number of signal's periods processed coherently, would have improved the post-coherent-integration SNR, resulting in the brighter intensity of the pixel in the target scattering display (see Figs. 3 and 4). It would also have decreased the Doppler (range-rate) width of the pixel. On the other hand, it would have increased the separation between target track points in Fig. 5, resulting in fewer measurements during the 2.4 s of target visibility. The track estimation algorithm can be considered an "incoherent integration". We can therefore conclude that increasing t_s increases coherent integration and decreases incoherent integration and vice versa.

Note that the pixel's delay (range) width is determined by the duration of an element (bit) in the phase-coded sequence that modulates the periodic CW signal. Reducing the range-width of the pixel requires a shorter bit duration, namely a wider signal bandwidth. Reducing the pixel's range-width (range resolution) may raise the problem of range migration [10]. To avoid range migration during the CPI ($= t_s = 0.05$ s) the product of the expected magnitude of the range-rate (70 m/s) times the CPI should be lower than the range resolution (3.75 m), which is indeed the case.

B. Brief Interpretation of Scattering Pattern

The target's range/range-rate scattering pattern (see Fig. 3) shows that the airliner target extends over many radar 2-D resolution pixels, in both BS dimensions (r and $\dot{r}$). That raises an obvious question—what does Fig. 3 tell us about the target's geometrical structure? An answer is far beyond the scope of this paper, but a hint can be obtained from Fig. 10, adopted from [11] and [12], which represents a Boeing 747 departing from Adelaide airport. The similarity between Figs. 3 and 10 points possible matches between the strong scatterers and the airliner components.

VII. DISCUSSION

The BS positioning approach, which enables all of the above, is possible because a distance d separates the transmitter from the receiver. The setting $d \rightarrow 0$ will take away those properties. Hence, it is reasonable to deduce that increasing d will improve the estimations accuracies. More

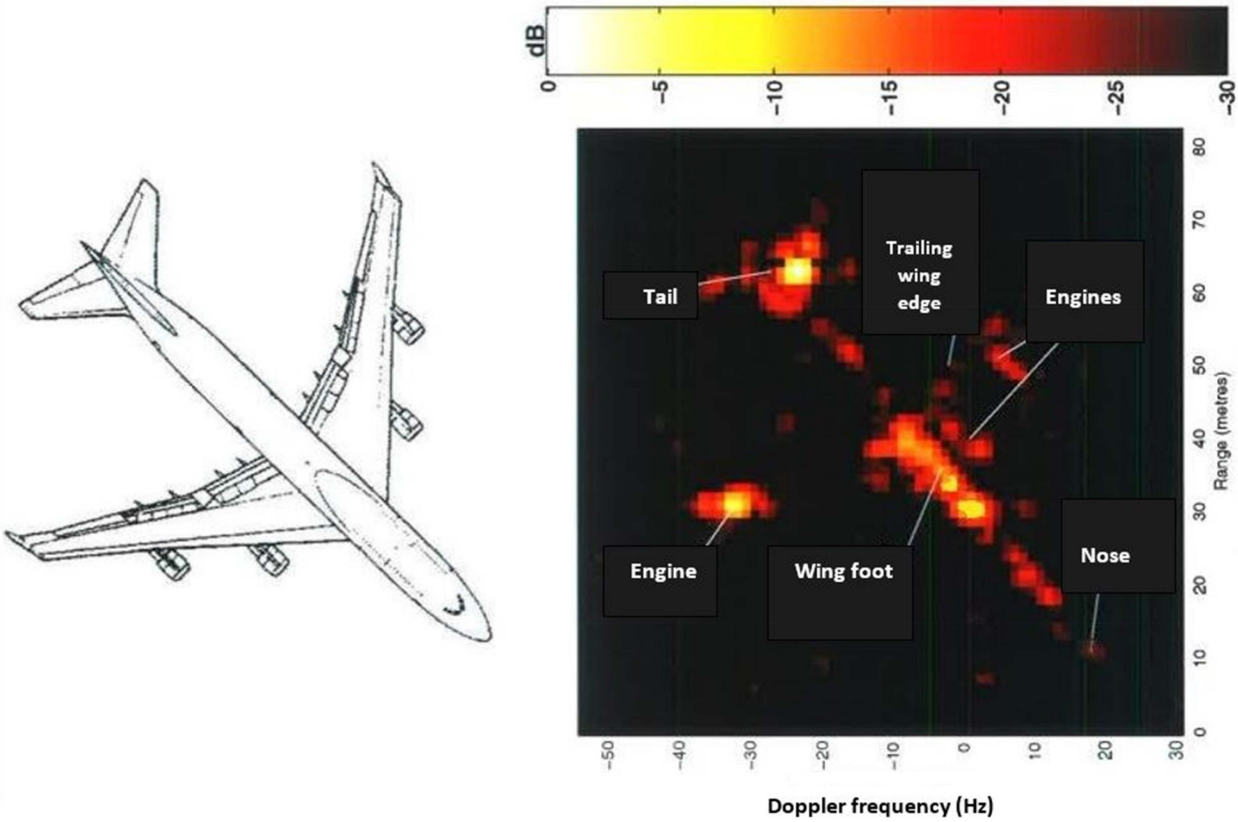

Fig. 10. ISAR image of an outgoing Boeing 747 aircraft. The image (from [11]) was generated from real data collected at Adelaide airport.

synthetic simulations, conducted but not shown, confirmed that assumption.

Regarding the fact that, in a 2-D scene, a range-rate measurement alleviates the requirement for more than one baseline, it may be worthwhile to point out the first author's experience in the design of the Globalstar satellite communication system [13], [14]. The availability of both *range* and *range-rate* measurements, between a single moving satellite and a (relatively) stationary user terminal (UT) on the Earth's surface, enabled satisfactory positioning of the UT when only one Globalstar satellite was in view. Help from the GPS system was added only years later. The Globalstar single-satellite positioning failed when the UT was near the satellite subtrack. There too (compare to Fig. 8) the iso-range circle and the iso-range-rate hyperbola created two close intersections, almost symmetrical on opposite sides of the satellite subtrack. In Globalstar, thanks to the Earth's rotation, for most locations on the globe, the symmetry was not perfect, providing a clue as to which intersection is true.

VIII. CONCLUSION

Using a field experiment and simulations, this article demonstrated how a coherent BS radar with one baseline, separating the transmitter and the receiver, could estimate the 2-D parameters of a moving target: location $(x,\ y)$ *and* velocity and heading direction $(v_x,\ v_y)$. The required measurements are a sequence of range and range-rate measurements taken along a short track of the target. The most appealing property is that direction measurements are not required! Unfavorable scenes are cases in which the target heads toward, or away from, the baseline's center, which results in poor GDOP. If the altitude h, of the target above the horizontal plain, joins the list of estimated parameters, the geometry becomes 3-D, and a second receiver is required. The obvious next candidate to be added to the list of unknowns is the target's vertical velocity v_h.

REFERENCES

[1] I. Cohen, R. Elster, and N. Levanon, "Good bistatic continuous waveform for active bistatic radar," *IET Radar, Sonar Navigat.*, vol. 10, no. 4, pp. 798–806, 2016.

[2] M. Inggs, H. Griffiths, F. Fioranelli, M. Ritchie, and K. Woodbridge, "Multistatic radar: System requirements and experimental validation," in *Proc. Int. Radar Conf.*, 2014, pp. 1–6.

[3] B. Fan, F. Zhang, C. Ma, Y. Yang, S. Pan, and X. Wang, "Microwave photonic bistatic radar for real-time and high resolution imaging," *IEEE Photon. Technol. Lett.*, vol. 32, no. 21, pp. 1397–1400, Nov. 2020.

[4] T. Johnsen and K. E. Olsen, "Bi- and multistatic radar," in *Proc. Adv. Radar Signal Data Process.*, 2006, pp. 4-1–4-34. [Online]. Available: https://www.sto.nato.int/publications/STOEducationalNotes/RTO-EN-SET-086/EN-SET-086-04.pdf

[5] F. D. V. Maasdorp, "Doppler-only target tracking for a multistatic radar exploiting FM band illumination of opportunity," PhD. thesis, Dept. Elect. Eng., Univ. Cape Town, Cape Town, South Africa, Dec. 2015. [Online]. Available: https://open.uct.ac.za/bitstream/handle/11427/16550/thesis_ebe_2015_maasdorp_francois_de_villiers.pdf?sequence=1&isAllowed=y

[6] G. Manfredi et. al., "Measurements and analysis of the Doppler signature of a human moving within the forest in UHF-band," *Remote Sens.*, vol. 13, no. 3, 2021, Art. no. 423. [Online]. Available: https://doi.org/10.3390/rs13030423
[7] E. R. Swanson, "Geometric dilution of precision," *Navigation*, vol. 25, no. 4, pp. 425–429, 1979.
[8] R. B. Langley, "Dilution of precision," *GPS World*, vol. 10, no. 5, pp. 52–59, May 1999.
[9] J. Holden, *Angle-of-Arrival Estimation Using Radar Interferometry*. Edison, NJ, USA: Scitech Publishing, 2014.
[10] P. Jin, X. Rao, X. Zhu, and F. Kan, "Weak target integration detection based on bistatic radar second-order keystone transform," in *Proc. IEEE Int. Conf. Signal Inf. Data Process.*, 2019, pp. 1–6.
[11] A. Zyweck and R. E. Bogner, "Radar target classification of commercial aircraft," *IEEE Trans. Aerosp. Electron. Syst.*, vol. 32, no. 2, pp. 598–606, Apr. 1996.
[12] A. Zyweck, "Preprocessing issues in high resolution radar target classification," Ph.D. thesis, Fac. Eng., Dept. Elect. Electron. Eng., Univ. Adelaide, Adelaide, SA, Australia, Mar. 1995. [Online]. Available: https://digital.library.adelaide.edu.au/dspace/bitstream/2440/18524/2/02whole.pdf
[13] N. Levanon, "Quick position determination using 1 or 2 LEO satellites," *IEEE Trans. Aerosp. Electron. Syst.*, vol. 34, no. 3, pp. 736–754, Jul. 1998.
[14] N. Levanon, "Instant active positioning with one LEO satellite," *Navigation*, vol. 46, no. 2, pp. 87–95, 1999.

Itzik Cohen was born in Israel, in 1981. He received the B.Sc. (Hons.) degree in physics and the M.Sc. degree in electrical engineering in 2010 and 2016, respectively, from Tel Aviv University, Tel Aviv, Israel, where he is currently working toward the Ph.D. degree in electrical engineering.

Between 2000 and 2007, he was in the Israeli army. From 2007 to 2015, he was with Elbit Systems, Haifa, Israel.

Mr. Cohen was recipient of the Weinstein prize for a scientific publication in the field of signal processing (2016) and the Weinstein prize for excellence in studies (2017).

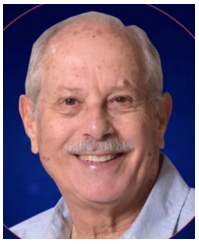

Nadav Levanon (Life Fellow, IEEE) received his B.Sc. and M.Sc. degrees from the Technion, Haifa, Israel, in 1961 and 1965, and the Ph.D. degree from the University of Wisconsin, Madison, WI, USA, in 1969, all in Electrical Engineering. He is a Professor Emeritus at Tel Aviv University, Tel Aviv, Israel, where he has been a faculty member since 1970. His books are *Radar Principles* (Wiley, 1988), *Radar Signals* (Wiley, 2004), *Radar – Concise Course*, vols. 1 and 2 (open access, 2021).

Prof. Levanon's 1998 IEEE Fellow citation is for "Contribution to radar signal analysis and detection." In 2016, he was the recipient of the IEEE Dennis J. Picard medal for Radar Technology and Applications, cited for "Contributions to radar signal design and analysis, pulse compression, and signal processing."